Energy & Environmental Science

PAPER

View Article Online
View Journal | View Issue

Cite this: *Energy Environ. Sci.*, 2017, **10**, 377

Solar hydrogen production using epitaxial $SrTiO_3$ on a GaAs photovoltaic†

L. Kornblum,‡[ab] D. P. Fenning,‡[cd] J. Faucher,‡[e] J. Hwang,[f] A. Boni,[cg] M. G. Han,[h] M. D. Morales-Acosta,[ab] Y. Zhu,[h] E. I. Altman,[bi] M. L. Lee,[ek] C. H. Ahn,[abj] F. J. Walker§*[ab] and Y. Shao-Horn§*[cf]

Received 28th October 2016,
Accepted 22nd December 2016

DOI: 10.1039/c6ee03170f

www.rsc.org/ees

We demonstrate an oxide-stabilized III–V photoelectrode architecture for solar fuel production from water in neutral pH. For this tunable architecture we demonstrate 100% Faradaic efficiency for hydrogen evolution, and incident photon-to-current efficiencies (IPCE) exceeding 50%. High IPCE for hydrogen evolution is a consequence of the low-loss interface achieved *via* epitaxial growth of a thin oxide on a GaAs solar cell. Developing optimal energetic alignment across the interfaces of the photoelectrode using well-established III–V technology is key to obtaining high performance. This advance constitutes a critical milestone towards efficient, unassisted fuel production from solar energy.

Introduction

One of the grand challenges for creating a sustainable society is to develop practical materials and devices that produce fuels when exposed to sunlight. Solar fuel production, *e.g. via* photoelectrochemical (PEC) water splitting[1–3] or CO_2 reduction,[4,5] allows the storage of solar energy in chemical bonds for use on demand. Transition metal oxides[6,7] represent a flexible class of materials for promoting water splitting kinetics including hydrogen and oxygen evolution from water, but unfortunately their bandgaps are typically too wide for efficient solar energy collection. Meanwhile, the most efficient solar energy collectors, III–V semiconductor solar cells,[8] are not chemically stable in the relevant environments for long term operation.[9,10]

Recent advances in photoelectrochemical hydrogen[11] and oxygen evolution[2,12–14] include the incorporation of III–V semiconductor solar cells,[15,16] stabilized using surface protection oxides,[11,17] phosphides and sulfides;[18] often in combination with precious metal catalysts, *e.g.*, Pt,[11,17,19,20] to promote reaction kinetics. For example, ground breaking work using InP semiconductors[21,22] achieved high efficiency using a protective oxide formed by chemical reaction of the semiconductor and electrolyte, followed by application of a precious metal catalyst. Further advances toward the development of more robust catalyst-oxide-semiconductor heterostructures can be made using an epitaxial oxide where each interface can be engineered to achieve catalytic activity without a precious metal and to provide robust protection from the electrolyte. In addition, incomplete control of the interfaces between the catalysts, surface protection layers, and the underlying semiconductor, has limited the ability to achieve further advances.[23] Here, we demonstrate a stable, epitaxial oxide III–V photoelectrode architecture for solar fuel production from water in neutral pH. For this tunable architecture we demonstrate 100% Faradaic efficiency for hydrogen evolution, and incident photon-to-current efficiencies (IPCE) exceeding 50%. The high IPCE is a consequence of the low-loss interface achieved *via* epitaxial growth of a thin oxide on a GaAs solar cell with a band offset that promotes electron transfer to the hydrogen reduction couple. The $SrTiO_3$ forms a single

[a] *Dept. of Applied Physics, Yale University, New Haven, CT 06511, USA. E-mail: fred.walker@yale.edu*
[b] *Center for Research on Interface Structures and Phenomena, Yale University, New Haven, CT 06511, USA*
[c] *Dept. of Mechanical Engineering, Massachusetts Institute of Technology, Cambridge, MA 02139, USA. E-mail: shaohorn@mit.edu*
[d] *Dept. of Nanoengineering, University of California San Diego, La Jolla, CA 92093, USA*
[e] *Dept. of Electrical Engineering, Yale University, New Haven, CT 06511, USA*
[f] *Dept. of Materials Science and Engineering, Massachusetts Institute of Technology, Cambridge, MA 02139, USA*
[g] *Dept. of Chemistry "G. Ciamician", University of Bologna, via Selmi 2, 40126 Bologna, Italy*
[h] *Condensed Matter Physics and Materials Science Dept., Brookhaven National Laboratory, Upton, NY 11973, USA*
[i] *Dept. of Chemical Engineering and Environmental Engineering, Yale University, New Haven, CT 06511, USA*
[j] *Dept. of Mechanical Engineering & Materials Science, Yale University, New Haven, CT 06511, USA*
[k] *Department of Electrical and Computer Engineering, University of Illinois at Urbana-Champaign, Urbana, IL 61801, USA*

† Electronic supplementary information (ESI) available: Details of experimental methods, solar cell growth, photovoltaic characteristics, molecular beam epitaxy, structural and electronic characterization of the oxide–semiconductor interface, photoelectrochemical measurements, oxide stability characterization, and trace impurity analysis. See DOI: 10.1039/c6ee03170f

‡ Equal contribution.

§ Equal contribution.

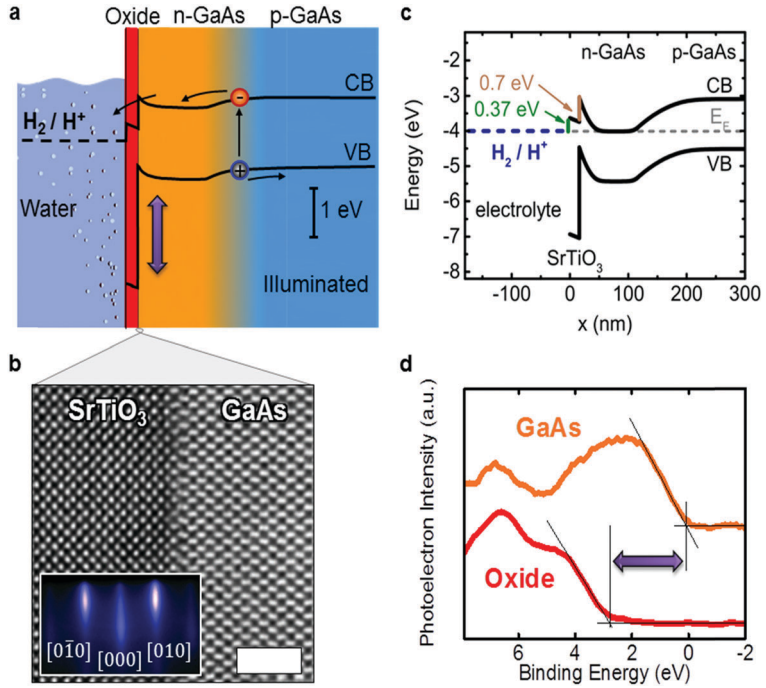

Fig. 1 Physical and electronic structure of the photocathode consisting of an epitaxial oxide grown on a semiconductor solar cell. (a) Schematic of the 16 nm-thick $SrTiO_3$/np-GaAs(001) photocathode (STOPC) at 0 V_{RHE} under illumination, where sunlight is absorbed in the semiconductor solar cell, generating a voltage and driving electrons to the oxide–water interface for hydrogen evolution. CB and VB denote the conduction and valence bands, respectively. (b) The atomic structure of the $SrTiO_3$/n-GaAs(001) interface using high-angle annular dark-field imaging (2 nm scale bar), and RHEED of the $SrTiO_3$ surface taken along the [100] direction after growth (inset). (c) The proposed energy alignment at the water/$SrTiO_3$ and $SrTiO_3$/GaAs(001) interfaces in equilibrium with the H^+/H_2 couple. (d) X-ray photoelectron spectra of the valence band offset (horizontal arrow) at the $SrTiO_3$/n-GaAs(001) interface (vertical arrow in panel a).

crystal, epitaxial layer with an atomically abrupt interface with the GaAs so that the electron energetics can be traced in detail from electron–hole pair generation in the GaAs to the efficient delivery of the electron to a hydrogen ion at the $SrTiO_3$–electrolyte interface.

We report an np-GaAs(001) photocathode that operates in neutral pH, stabilized by an epitaxial $SrTiO_3$ surface layer to deliver 3.1 mA cm^{-2} of hydrogen evolution current at 0.18 V above the thermodynamic potential. The photocathode consists of a 16 nm-thick single-crystal $SrTiO_3$ layer that protects the GaAs photocathode and provides stability during 24+ hours of hydrogen production. IPCE measurements reveal little loss of photogenerated carriers at the atomically-sharp $SrTiO_3$/np-GaAs(001) interface, permitting electron flow to the surface with a large thermodynamic driving force for hydrogen evolution reaction (HER, Fig. 1a). By achieving a quantitative description of the electronic band alignment at both the electrolyte–oxide interface and the buried oxide–semiconductor interface, we demonstrate the potential for this epitaxial oxide–semiconductor platform to leverage both oxide[24] and III–V band-engineering[25] toward highly efficient photoelectrochemical devices.

While photoelectrochemical water-splitting at extreme pH is currently preferred,[26] neutral pH operation remains an important goal for environmentally-benign solar fuels.[27,28] At the system level, the water splitting in extreme alkaline or acidic environments is important for limiting transport and concentration polarization.[29,30] More fundamentally, extreme pH conditions enhance the activity of catalytic surfaces currently available. We also note that perovskite surfaces offer promising opportunities for CO_2 reduction, which operates preferentially in near-neutral pH.[31] Enhancing the activity of available surfaces, especially at neutral pH, is a fundamental challenge for the field and addressed in this work. The fundamental aspects of interfaces and band alignments presented here will enable the integration of oxide electronic materials and III–V semiconductors for efficient solar fuel production.

Results and discussion

A thin $SrTiO_3$ metal oxide layer of 40 unit cells (~16 nm-thick) is epitaxially grown[32] on GaAs(001) solar cells by molecular beam epitaxy (MBE). A schematic of the 16 nm-thick $SrTiO_3$/np-GaAs(001) photocathode (STOPC) operating under illumination at 0 V *vs.* the reversible hydrogen electrode (RHE), or 0 V_{RHE} is shown in Fig. 1a. The np-GaAs(001) solar cells (Table S1 and Fig. S1, ESI†) consist of an np junction with a p-$Al_{0.4}Ga_{0.6}As$ back surface field with a measured open-circuit voltage of 0.94 V (Fig. S2, ESI†). The np junction separates photoexcited electrons and holes and the electrons flow through the conduction band to the $SrTiO_3$ surface where they reduce protons to hydrogen; in addition, the wide $SrTiO_3$ bandgap blocks holes

from reaching the surface. The MBE growth of the oxide results in an atomically sharp interface between $SrTiO_3$ and GaAs(001) as confirmed by scanning transmission electron microscopy (Fig. 1b). Streaks in the reflection high-energy electron diffraction (RHEED) indicate a smooth $SrTiO_3$ surface with high crystallinity (Fig. 1b, inset). High-quality crystalline (Fig. S3 and S4, ESI†) interfaces provide a platform for understanding and band engineering of oxide III–V photocathodes.

The proposed band alignments at the $SrTiO_3$/GaAs(001) and water–$SrTiO_3$ interfaces in the dark at equilibrium with the H^+/H_2 couple (0 V_{RHE} and −4.0 eV on the absolute energy scale at pH 7) are shown in Fig. 1c. X-ray photoelectron spectroscopy (XPS) analysis of the valence band (Fig. 1d) and As 3d and Ti 3p core levels (Fig. S5, ESI†) places the $SrTiO_3$ conduction band[33] 0.7 ± 0.2 eV below that of GaAs. When the electron energy equilibrates with the H^+/H_2 couple, this alignment also causes the GaAs bands at the interface with $SrTiO_3$ to bend upwards, forming a barrier for electron transport to the $SrTiO_3$ conduction band (Fig. 1c). Under illumination (Fig. 1a), a portion of the photovoltage of the solar cell is needed to reduce the magnitude of this barrier and produce HER current. In addition, the valence band of $SrTiO_3$ is positioned 2.6 ± 0.2 eV below that of n-GaAs, providing a large hole-blocking barrier that prevents hole transport from the n-GaAs into $SrTiO_3$ and GaAs corrosion.[9] The $SrTiO_3$ conduction band edge is 0.37 eV higher than energy of the hydrogen on the absolute scale (Fig. 1c), as determined from the Mott–Schottky analysis of the flatband potential of a conductive, 1 (at)% Nb-doped $SrTiO_3$ single crystal (Fig. S6, ESI†). The doping induces negligible changes to the optical gap from that of undoped $SrTiO_3$[34] and is a good approximation to the epitaxial $SrTiO_3$. Fast HER kinetics can be expected given the large 0.37 eV thermodynamic driving force.[35,36]

Electrochemical HER measurements were performed on 5 × 5 mm^2 pieces of this structure, which were contacted on the backside and insulated from the sides to form the photocathode. Photoelectrochemical HER kinetics were measured in 0.1 M potassium phosphate electrolyte solution (pH 7), selected for its non-corrosive, non-toxic buffering.[37] While similar $SrTiO_3$ films have exhibited excellent stability under acidic conditions,[11] a neutral pH chemistry was chosen to provide an environmentally-benign, non-hazardous route for HER.

Because of the band alignments in the STOPC, large solar-to-hydrogen currents are realized under 1 Sun, and the catalyst-free STOPC provides a ∼0.55 V voltage gain with respect to a Pt catalyst after extended chronoamperometry (at 1 mA cm^{-2}, Fig. 2a). Following 24 h solar hydrogen production at 0 V_{RHE} under simulated 1 Sun illumination, cyclic voltammetry of the STOPC shows a HER onset potential of ∼0.3 V_{RHE}, and a large reduction current of 6 mA cm^{-2} at 0 V_{RHE} (Fig. 2a). Bubble formation and mass transport limitations are observed as noise in the current measurement below 0.1 V_{RHE} (Fig. 2a). Gas chromatography measurements show that hydrogen evolution accounts for all the measured reduction current, yielding ∼100% Faradaic efficiency (Fig. 2b). Comparing this onset potential to the V_{oc} of 0.94 V highlights the prospects for further improvements accessible in this material system.

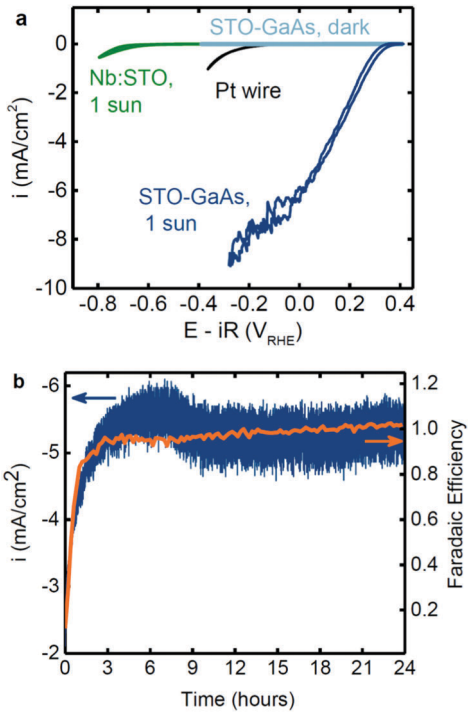

Fig. 2 Photoelectrochemical performance and stability of the $SrTiO_3$-GaAs photocathode. (a) Cyclic voltammograms (CV) of hydrogen evolution currents from $SrTiO_3$/np-GaAs photocathode in the dark and under 1 simulated Sun compared with those of 1 (at)% Nb-doped $SrTiO_3$ and Pt wire after 24 h chronoamperometry at −0.4 V_{RHE}. The photovoltage generated by the np-GaAs solar cell shifts the onset potential of HER to positive voltage for the $SrTiO_3$–GaAs photocathode. (b) Stability during a 24 h CA measurement of the $SrTiO_3$/np-GaAs photocathode, overlaid with the efficiency calculated from gas chromatography.

In contrast to the illuminated photocathode, the reduction current is negligible on the $SrTiO_3$/np-GaAs in dark even at −0.4 V_{RHE}. An illuminated Nb:$SrTiO_3$-(001) photoelectrode that can only collect UV light[34,38] produces negligible currents at 0 V_{RHE}, and dark reduction currents become measureable at potentials below −0.8 V_{RHE}. The large reduction current and gain in potential measured under illumination for the $SrTiO_3$–GaAs result from electrons generated by the III–V solar cell that are injected into the $SrTiO_3$ conduction band and reduce protons to hydrogen at the oxide surface.

HER currents from the STOPC remained stable under 1 Sun illumination during 24 h potentiostatic testing at 0 V_{RHE}, as shown in Fig. 2b. A second round of CV and IPCE measurements, performed at reaction conditions for several hours following chronoamperometry (CA) demonstrates that the STOPC stability extends beyond 24 h. The increase in reduction current at short times during chronoamperometry (0–2 hours) and improvement in CV measurements (Fig. S7, ESI†) is consistently observed for all $SrTiO_3$/np-GaAs samples, and suggests an activation of the $SrTiO_3$/electrolyte interface. After 24 hours of operation under simulated sunlight, XPS analysis shows negligible changes in the $SrTiO_3$ surface chemistry (Fig. S8, ESI†). In contrast, bare np-GaAs photoelectrodes quickly corrode under these conditions (Fig. S9, ESI†). We thus demonstrate that 16 nm-thick epitaxial $SrTiO_3$

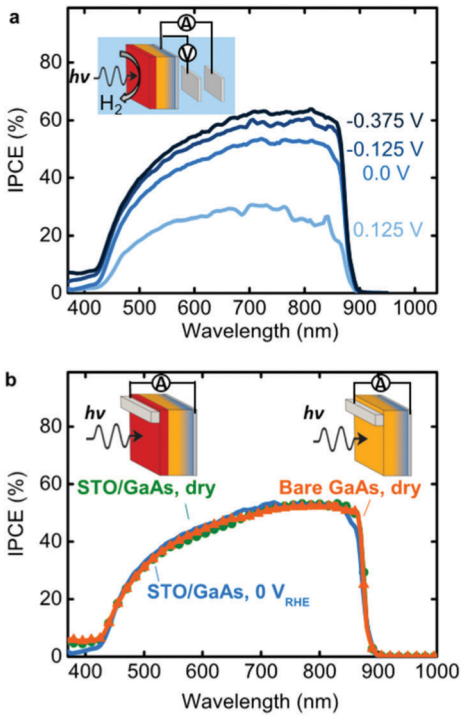

Fig. 3 Spectral response of $SrTiO_3$/np-GaAs devices. (a) Incident photon-to-current efficiency (IPCE) in solution at different potentials near 0 V_{RHE}. (b) IPCE of two-contact photovoltaic measurements with no electrolyte with and without $SrTiO_3$ compared to IPCE of photoelectrochemical HER at 0 V_{RHE} (from panel a). Insets show schematics of measurement configurations.

provides sustainable chemical protection and passivation to the underlying semiconducting solar cell.

Comparing the probability that incident photons lead to electrons collected at the cathode (IPCE) of the STOPC in solution where H_2 is generated (Fig. 3a) and in a photovoltaic configuration (Fig. 3b) reveals several important insights. First, in the photovoltaic configuration (Fig. 3b), the oxide has no impact on the GaAs IPCE which exceeds 50% between 700–850 nm. We further note that the similarity of the dry and PEC IPCE behaviour means that the reduction in the AM1.5g photocurrent in Fig. 2 relative to the photocurrent measured for the dry cell is not due to carrier recombination at the $SrTiO_3$/GaAs interface. Rather, the current reduction is the result of an effective series resistance due to the barrier at the $SrTiO_3$/GaAs interface (Fig. S14, ESI†) and kinetic limitations at the $SrTiO_3$/electrolyte interface.[39,40] Front surface reflectivity is responsible for much of the loss of incident photons,[41] thus nearly all the photoexcited electrons make it to the $SrTiO_3$ surface. At 0 V_{RHE}, Fig. 3a shows that the IPCE for H_2 generation is virtually identical to the photovoltaic IPCE, confirming robust electron transport from the $SrTiO_3$ surface to the electrolyte for H^+ reduction. The voltage dependence of the H_2 generation IPCE suggests barriers to charge injection into the electrolyte.

Unlike previous work on protected Si or GaAs photocathodes that requires the use of Pt,[11] the STOPC shows efficient carrier collection for hydrogen evolution without an additional metal catalyst. In order to rule out the impact of trace metal impurities such as platinum, on the catalytic performance of the photocathode device during PEC, an extended PEC and XPS study was conducted (Fig. S10–S13, ESI†). The conclusion from these studies is that the activity of the $SrTiO_3$ surface cannot be attributed to surface Pt contamination. The IPCE values demonstrated here (Fig. 3) are comparable to those of oxide-protected Si photocathodes[11] that required nano-structured Pt catalyst at a much higher overpotential of -0.4 V_{RHE}. Moreover, the addition of $\sim$3 nm of Pt on top of $SrTiO_3$/np-GaAs photocathode did not lead to significant changes in the hydrogen evolution current and IPCE. The large electronic driving force ($\sim$0.37 eV) for electron transfer from the oxide conduction band to the hydrogen–water redox couple is shown to be sufficient to promote hydrogen evolution kinetics.

Photoelectrochemical IPCE of the STOPC is comparable to photovoltaic (PV) IPCE of bare np-GaAs solar cells and is not reduced by the addition of the epitaxial oxide and the collection of current *via* HER instead of a metal contact (Fig. 3b). The IPCE at 0 V_{RHE} is in excellent agreement with the short-circuit dry two-contact PV IPCE. We expect that there is substantial opportunity for further gains in solar-to-hydrogen efficiency by improvements in the GaAs cell design.[42]

Energy losses at the $SrTiO_3$/n-GaAs and water–$SrTiO_3$ interfaces (Fig. 1c) lead to a reduction in the ratiometric power saved of the photoelectrode, which can be defined as the ratio of HER current times the HER potential relative to RHE to solar energy input.[20] As the most conservative estimate, the ratiometric power saved compared to an ideally nonpolarizable dark electrode (E = 0 V RHE) was used in part because our scheme is blocking for electron flow in the dark and exhibits a lack of superposition (Fig. S14, ESI†). This efficiency, calculated from Fig. 2a at the maximum power point to be $\sim$0.55%, is reduced from the maximum available from the solar cell, $\sim$10%. If there were no conduction band offset at the $SrTiO_3$/n-GaAs interface, the 0.94 V open-circuit voltage of the solar cell could shift the onset potential from the -0.37 V_{RHE} flatband of the $SrTiO_3$ in dark to $\sim$0.57 V_{RHE} under illumination. Due to the loss of electron energy at the conduction band offset between $SrTiO_3$ and GaAs (see Fig. S14 and S15, ESI†), the current device achieves an onset at $\sim$0.30 V_{RHE} (Fig. 2a). Thus, $\sim$0.27 V could be gained by tuning the interface chemistry to reduce the conduction band offset using functional oxide engineering techniques applicable to epitaxial oxides like $SrTiO_3$ or by creating a thin heavily-doped tunnelling layer of n^+-GaAs at the interface. Several hundred mV of further improvement could be gained by reducing the 0.37 V offset at the water–oxide interface by adjusting the oxide's band structure[43] to increase the electron affinity just enough so that some offset at the water–oxide interface remains to drive hydrogen evolution without a catalyst. The quantitative band alignments developed here outline a clear path toward greater photoelectrode efficiency.

Conclusions

This work demonstrates the robustness of integrating III–V technology with a high-quality single-crystal, epitaxial oxide as

a platform for further development of photocathodes for solar fuel production. Using a catalyst-free 16 nm-thick $SrTiO_3$ on np-GaAs, a stable hydrogen evolution current is produced under 1 Sun with IPCE reaching 50% at the thermodynamic potential of 0 V_{RHE}. Because of the high-quality of the $SrTiO_3$/GaAs interface, the IPCE for hydrogen production matches the photovoltaic performance of the GaAs solar cell. Extending this approach to high-efficiency tandem solar cells offers the potential to generate sufficient photovoltage for stable unassisted water splitting. For example, a III–V on a Si dual-junction cell operating as a photocathode could achieve photovoltages well in excess of the 1.23 V thermodynamic minimum required for water-splitting while leveraging low-cost Si substrates with high efficiency III–V materials.[44,45] Combining the tunability of complex oxides and the sophisticated engineering of III–V solar cells, large gains in solar hydrogen production should be readily accessible using the catalyst-free oxide-stabilized III–V platform demonstrated here.

Acknowledgements

The authors (CHA, LK, MDAM, and FJW) acknowledge support from NSF DMR1309868 and EIA acknowledges support from MRSEC DMR-1119826 (CRISP). Support for MIT research is acknowledged from the MIT Energy Initiative seed fund and the Cooperative Agreement between the Masdar Institute of Science and Technology, Abu Dhabi, UAE and MIT, Reference Number 02/MI/MIT/CP/11/07633/GEN/G/00. DPF acknowledges the support of the MIT/Battelle postdoctoral program. JF and MLL acknowledge support from ARPA-E Award DE-AR0000508. The work at Brookhaven National Laboratory was supported by the Materials Science and Engineering Divisions, Office of Basic Energy Sciences, of the US Department of Energy, under Contract No. DE-AC02-98CH10886. The authors are grateful to Nir Pour for his expertise in preparing Fig. 1. The authors also thank Dr Ifan E. L. Stephens for discussions and assistance in measuring Pt wire, and Dr B. R. Lukanov for his contributions to the early stages of this project.

References

1 A. Fujishima and K. Honda, *Nature*, 1972, **238**, 37–38.
2 S. Hu, M. R. Shaner, J. A. Beardslee, M. Lichterman, B. S. Brunschwig and N. S. Lewis, *Science*, 2014, **344**, 1005–1009.
3 S. C. Warren, K. Voïtchovsky, H. Dotan, C. M. Leroy, M. Cornuz, F. Stellacci, C. Hébert, A. Rothschild and M. Grätzel, *Nat. Mater.*, 2013, **12**, 842–849.
4 M. Schreier, L. Curvat, F. Giordano, L. Steier, A. Abate, S. M. Zakeeruddin, J. Luo, M. T. Mayer and M. Gratzel, *Nat. Commun.*, 2015, **6**, 7326.
5 F. Studt, I. Sharafutdinov, F. Abild-Pedersen, C. F. Elkjær, J. S. Hummelshøj, S. Dahl, I. Chorkendorff and J. K. Nørskov, *Nat. Chem.*, 2014, **6**, 320–324.
6 R. B. Comes, S. Y. Smolin, T. C. Kaspar, R. Gao, B. A. Apgar, L. W. Martin, M. E. Bowden, J. B. Baxter and S. A. Chambers, *Appl. Phys. Lett.*, 2015, **106**, 092901.
7 C.-B. Eom and J. L. MacManus-Driscoll, *APL Mater.*, 2015, **3**, 062201.
8 M. A. Green, K. Emery, Y. Hishikawa, W. Warta and E. D. Dunlop, *Prog. Photovoltaics Res. Appl.*, 2015, **23**, 1–9.
9 H. Gerischer, *J. Electroanal. Chem. Interfacial Electrochem.*, 1977, **82**, 133–143.
10 O. Khaselev and J. A. Turner, *Science*, 1998, **280**, 425–427.
11 L. Ji, M. D. McDaniel, S. Wang, A. B. Posadas, X. Li, H. Huang, J. C. Lee, A. A. Demkov, A. J. Bard, J. G. Ekerdt and E. T. Yu, *Nat. Nanotechnol.*, 2015, **10**, 84–90.
12 C. R. Cox, J. Z. Lee, D. G. Nocera and T. Buonassisi, *Proc. Natl. Acad. Sci. U. S. A.*, 2014, **111**, 14057–14061.
13 M. J. Kenney, M. Gong, Y. Li, J. Z. Wu, J. Feng, M. Lanza and H. Dai, *Science*, 2013, **342**, 836–840.
14 Y. W. Chen, J. D. Prange, S. Dühnen, Y. Park, M. Gunji, C. E. D. Chidsey and P. C. McIntyre, *Nat. Mater.*, 2011, **10**, 539–544.
15 E. Verlage, S. Hu, R. Liu, R. J. R. Jones, K. Sun, C. Xiang, N. S. Lewis and H. A. Atwater, *Energy Environ. Sci.*, 2015, **8**, 3166.
16 M. Malizia, B. Seger, I. Chorkendorff and P. C. K. Vesborg, *J. Mater. Chem. A*, 2014, **2**, 6847.
17 B. Seger, T. Pedersen, A. Laursen, P. Vesborg, O. Hansen and I. Chorkendorff, *J. Am. Chem. Soc.*, 2013, **135**, 1057–1064.
18 A. B. Laursen, T. Pedersen, P. Malacrida, B. Seger, O. Hansen, P. C. K. Vesborg and I. Chorkendorff, *Phys. Chem. Chem. Phys.*, 2013, **15**, 20000–20004.
19 H.-P. Wang, K. Sun, S. Y. Noh, A. Kargar, M.-L. Tsai, M.-Y. Huang, D. Wang and J.-H. He, *Nano Lett.*, 2015, **15**, 2817–2824.
20 S. W. Boettcher, E. L. Warren, M. C. Putnam, E. a. Santori, D. Turner-Evans, M. D. Kelzenberg, M. G. Walter, J. R. McKone, B. S. Brunschwig, H. a. Atwater and N. S. Lewis, *J. Am. Chem. Soc.*, 2011, **133**, 1216–1219.
21 A. Heller, *Science*, 1984, **223**, 1141–1148.
22 M. H. Lee, K. Takei, J. Zhang, R. Kapadia, M. Zheng, Y.-Z. Chen, J. Nah, T. S. Matthews, Y.-L. Chueh, J. W. Ager and A. Javey, *Angew. Chem., Int. Ed.*, 2012, **51**, 10760–10764.
23 C. R. Cox, M. T. Winkler, J. J. H. Pijpers, T. Buonassisi and D. G. Nocera, *Energy Environ. Sci.*, 2013, **6**, 532–538.
24 R. A. McKee, F. J. Walker and M. F. Chisholm, *Science*, 2001, **293**, 468–471.
25 R. M. France, J. F. Geisz, M. A. Steiner, W. E. Mcmahon, D. J. Friedman, T. E. Moriarty, C. Osterwald, J. S. Ward, A. Duda, M. Young and W. J. Olavarria, *IEEE J. Photovoltaics*, 2015, **5**, 432–437.
26 J. Jin, K. Walczak, M. R. Singh, C. Karp, N. S. Lewis and C. Xiang, *Energy Environ. Sci.*, 2014, **7**, 3371–3380.
27 B. J. Trześniewski and W. A. Smith, *J. Mater. Chem. A*, 2016, **4**, 2919–2926.
28 Q. Wang, T. Hisatomi, Q. Jia, H. Tokudome, M. Zhong, C. Wang, Z. Pan, T. Takata, M. Nakabayashi, N. Shibata,

Y. Li, I. D. Sharp, A. Kudo, T. Yamada and K. Domen, *Nat. Mater.*, 2016, **15**, 611–615.
29 C. Xiang, K. M. Papadantonakis and N. S. Lewis, *Mater. Horiz.*, 2016, **3**, 169–173.
30 M. R. Singh, K. Papadantonakis, C. Xiang and N. S. Lewis, *Energy Environ. Sci.*, 2015, **8**, 2760–2767.
31 Y. Hori, A. Murata, R. Takahashi and S. Suzuki, *Chem. Lett.*, 1987, 1665–1668.
32 R. Contreras-Guerrero, M. Edirisooriya, O. C. Noriega and R. Droopad, *J. Cryst. Growth*, 2013, **378**, 238–242.
33 S. A. Chambers, Y. Liang, Z. Yu, R. Droopad, J. Ramdani and K. Eisenbeiser, *Appl. Phys. Lett.*, 2000, **77**, 1662.
34 K. J. May, D. P. Fenning, T. Ming, W. T. Hong, D. Lee, K. A. Stoerzinger, M. D. Biegalski, A. M. Kolpak and Y. Shao-Horn, *J. Phys. Chem. Lett.*, 2015, **6**, 977–985.
35 J. K. Nørskov, T. Bligaard, A. Logadottir, J. R. Kitchin, J. G. Chen, S. Pandelov and U. Stimming, *J. Electrochem. Soc.*, 2005, **152**, J23–J26.
36 S. Trasatti, *Electrochim. Acta*, 1984, **29**, 1503–1512.
37 M. W. Kanan and D. G. Nocera, *Science*, 2008, **321**, 1072–1075.
38 K. Van Benthem, C. Elsässer and R. H. French, *J. Appl. Phys.*, 2001, **90**, 6156–6164.
39 A. G. Scheuermann, J. P. Lawrence, K. W. Kemp, T. Ito, A. Walsh, C. E. D. Chidsey, P. K. Hurley and P. C. McIntyre, *Nat. Mater.*, 2016, **15**, 99–105.
40 A. G. Scheuermann, C. E. D. Chidsey and P. C. McIntyre, *J. Electrochem. Soc.*, 2016, **163**, H192–H200.
41 D. E. Aspnes and A. A. Studna, *Phys. Rev. B: Condens. Matter Mater. Phys.*, 1983, **27**, 985–1009.
42 O. D. Miller, E. Yablonovitch and S. R. Kurtz, *IEEE J. Photovoltaics*, 2012, **2**, 303–311.
43 S. Yang, D. Prendergast and J. B. Neaton, *Nano Lett.*, 2012, **12**, 383–388.
44 S. Hu, C. Xiang, S. Haussener, A. D. Berger and N. S. Lewis, *Energy Environ. Sci.*, 2013, **6**, 2984–2993.
45 J. R. Lang, J. Faucher, S. Tomasulo, K. Nay Yaung and M. Larry Lee, *Appl. Phys. Lett.*, 2013, **103**, 092102.

